World Academy of Science, Engineering and Technology
International Journal of Electrical and Computer Engineering
Vol:3, No:5, 2009

Coherence Analysis between Respiration and PPG Signal by Bivariate AR Model

Yue-Der Lin, Wei-Ting Liu, Ching-Che Tsai, Wen-Hsiu Chen

***Abstract*—**PPG is a potential tool in clinical applications. Among such, the relationship between respiration and PPG signal has attracted attention in past decades. In this research, a bivariate AR spectral estimation method was utilized for the coherence analysis between these two signals. Ten healthy subjects participated in this research with signals measured at different respiratory rates. The results demonstrate that high coherence exists between respiration and PPG signal, whereas the coherence disappears in breath-holding experiments. These results imply that PPG signal reveals the respiratory information. The utilized method may provide an attractive alternative approach for the related researches.

***Keywords*—**Coherence analysis, photoplethysmography (PPG), bivariate AR spectral estimation.

I. Introduction

PHOTOPLETHYSMOGRAPHY (PPG) signal represents the volumetric changes in blood vessels. Such blood volume change occurs mainly in the arteries and arterioles. The principle of PPG is that the light (mainly red, infrared or green light) traveling through biological tissue (e.g. the fingertip or earlobe) will be absorbed by different absorbing substances, including skin pigmentation, bone, and arterial and venous blood. The arteries contain more blood during systole than during diastole, and their diameter increases due to the increased blood pressure. The detected light reflected from or transmitted through the vessels will thus fluctuate according to the pulsatile blood flow during the circulation. Therefore, the PPG signals are composed of two components, the alternating part of total absorbance due to the pulsatile component of the arterial blood (AC component) and the absorbance due to venous blood, the part of the constant amount of arterial blood, and other non-pulsatile components such as skin pigmentation (DC component) [1]. The simplest PPG sensor consists of a light source and a photo detector packaged in a compact plastic housing. The advantages of PPG include its easiness to set up, simple use and low cost. In addition, PPG has the ability to take measurement without having direct contact with the skin surface. For these advantages, the PPG technology has attracted much attention in clinical applications [2].

Heart rate (or pulse rate) and respiratory rate are two important vital signs, they are of great importance when critically ill adults and newborn infants are monitored. Clinical monitoring of heart rate is generally performed by counting QRS complexes of the electrocardiogram (ECG) per time unit. The respiratory rate is usually monitored by the transthoracic impedance plethysmography [3] or thermal technique [4]. As the AC component of PPG signal is synchronous with the heart beat and thus can be identified as a source of heart rate information. When properly shielded, PPG can be used in electrosurgery, which usually disables the ECG measurement. In addition to heart-synchronous variations, the PPG signal contains respiratory-induced intensity variations (RIIV) [5]-[6]. This modulation arises from respiratory-induced variations in venous return to the heart, caused by the alterations in intrathoracic pressure. A part of the respiratory-related fluctuations in perfusion also originates from the autonomous control of the peripheral vessels and is also synchronous with respiration. RIIV signal can be extracted from PPG by a bandpass filter (0.13-0.48 Hz) [7]-[9]. High coherence has been shown between RIIV and changes in tidal volume and respiratory rate [7]-[9]. These results imply PPG is a potential tool to acquire heart rate and respiratory rate simultaneously.

The relationship between RIIV and respiratory signal has been examined extensively in the past decades. However, little information has been published concerning the coherence between raw PPG signal and respiratory signal. As the RIIV may deviate with the varying respiratory rate, the fixed bandpass filter for PPG signal filtration may limit the accuracy of analysis in practical conditions, especially in deep (or slow) and fast breathing cases. The objective of the present study was to investigate whether such coherence exists between raw PPG signal and respiratory signal. The bivariate autoregressive (AR) spectral estimation method proposed by Morf et al. [10], which is termed as Vieira-Morf method in [11], was utilized for the coherence analysis under different breathing rates and the breath-holding state for 10 healthy subjects. The bivariate AR-based cross-spectral analysis demonstrated that raw PPG signal and respiration were coherent (magnitude-squared coherence > 0.5) at the respiratory frequency in the subjects studied, with changes in respiration leading to changes in PPG. No coherence was found in breath-holding cases for almost all subjects. The results of this study verify that there exists the

Yue-Der Lin is with the Department of Automatic Control Engineering and the Master Program of Biomedical Informatics and Biomedical Engineering, Feng Chia University, Taiwan (corresponding author, phone: +886-4-24517250 ext 3925; fax: +886-4-24519951; e-mail: ydlin@fcu.edu.tw).

Wei-Ting Liu and Ching-Che Tsai are with the Department of Automatic Control Engineering, Feng Chia University, Taiwan.

Wen-Hsiu Chen is with the Master Program of Biomedical Informatics and Biomedical Engineering, Feng Chia University, Taiwan.

corresponding respiratory component in spectrum of raw PPG signal. The results may provide another attractive approach to acquire the respiratory information from PPG without the need of filtering, in which case the raw PPG signal can be processed for further applications.

II. Methods and Materials

A. Subjects and Experiments

Ten healthy subjects (eight males and two females, non-smoker and with no prior history of cardiovascular disease) aged between 22 and 24 took part in the experiments after giving the informed consent. All subjects were asked to refrain from caffeine and alcoholic drink at least 4 hours before the experiments. All of the experiments were performed at the same university laboratory with the room temperature being maintained at about 25 degrees centigrade during the night time (from 9 to 11 pm). The subjects were required to have a resting period of at least 5 minutes under relaxation status before the experiment.

Each experiment included three stages classified by different respiratory rate (20 breaths/min, 12 breaths/min and holding the breath in order). Each stage was maintained at least one minute, and the intervals between stages were 5 minutes. Throughout the experiment, the subjects were seated in a comfortable chair with their right upper arm kept at the height of heart level. The breathing rate is controlled by the subjects with a clock for their timing reference. The breathing rate is not easy to fix at a constant, but it is controlled to an acceptable precision during the whole experiment.

B. Signal Measurement and Signal Analysis

The Multifunctional physiological data acquisition system MP30® (Biopac Inc.) was utilized for signal measurement. PPG signal (by module SS4LA, with 66.5-Hz lowpass filtering) and respiratory signal (by module SS6L, also with 66.5-Hz lowpass filtering) were collected simultaneously during each experimental stage. The PPG probe (SS4LA, with infrared wavelength 860 nm) was attached to the right index finger, whereas the respiratory signal was acquired by fast response thermistor (SS6L) and was put at the nostril during the measurement. The user friendly analysis package Biopac Student Lab® was used for the signal management, including the signal quality pre-screening, data storage and retrieval. The sampling frequency was 250 Hz. The signals were verified visually by a well-trained technician. A typical respiratory signal and PPG signal are shown in Fig. 1. If the signal quality was poor, the signal would be excluded from further analysis and the subject was asked to repeat the experiment once again.

C. Signal Analysis

The analysis was executed after the experiments were finished and approved. The source code for bivariate AR spectral estimation was developed in MATLAB® (MathWorks Inc.). The estimation method was originally developed by Morf et al. [10]. It is an expansion of single-channel Levinson recursion algorithm [12], and is briefly described as below.

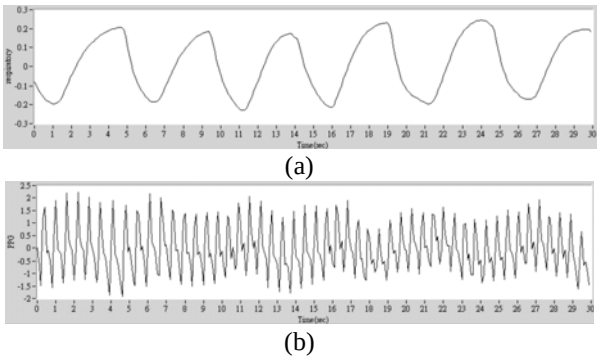

Fig. 1 Typical signals: (a) respiratory signal (12 breaths/min), (b) PPG signal

Let $\boldsymbol{x}[n]$ denote the vector of samples from two-channel process at sample index n

$$\boldsymbol{x}[n] = [x_1[n]\ \ x_2[n]]^T, \tag{1}$$

where the superscript ^{T} represent the transpose operation. In (1), $x_1[\cdot]$ and $x_2[\cdot]$ represent the acquired respiratory signal and PPG signal respectively, and both of them are all real-valued in this research. The bivariate AR(p) process, assumed to be wide-sense stationary (WSS), can be represented as

$$\boldsymbol{x}[n] = -\sum_{k=1}^{p} \boldsymbol{A}_p(k)\boldsymbol{x}[n-k] + \boldsymbol{e}_p^f[n], \tag{2}$$

for the forward AR process, or

$$\boldsymbol{x}[n-p-1] = -\sum_{k=1}^{p} \boldsymbol{B}_p(k)\boldsymbol{x}[n-p-1+k] + \boldsymbol{e}_p^b[n-1] \tag{3}$$

for the backward AR process. In (2) and (3), $\boldsymbol{A}_p(k)$ and $\boldsymbol{B}_p(k)$ are the 2×2 AR(p) forward and backward prediction parameter matrices, and $\boldsymbol{e}_p^f[n]$ and $\boldsymbol{e}_p^b[n-1]$ are the 2×1 vector representing the forward and backward prediction error of the AR(p) driving noise process. With the property that the driving noise process is uncorrelated with past values of the AR process, the two-channel Yule-Walker normal equations of forward linear prediction version can be derived as

$$\boldsymbol{a}_p \boldsymbol{R}_p = [\boldsymbol{P}_p^f\ \ \boldsymbol{0} \cdots \boldsymbol{0}], \tag{4}$$

in which

$$\boldsymbol{a}_p = [\boldsymbol{I}\ \boldsymbol{A}_p(1) \cdots \boldsymbol{A}_p(p)], \tag{5}$$

$$\boldsymbol{R}_p = E\{\boldsymbol{x}_p[n]\boldsymbol{x}_p^H[n]\}, \tag{6}$$

with

$$\boldsymbol{x}_p[n] = \begin{bmatrix} \boldsymbol{x}[n] \\ \boldsymbol{x}[n-1] \\ \vdots \\ \boldsymbol{x}[n-p] \end{bmatrix}, \tag{7}$$

and

$$\boldsymbol{P}_p^f = E\{\boldsymbol{e}_p^f[n]\boldsymbol{e}_p^{fH}[n]\}. \tag{8}$$

In the above equations, $\boldsymbol{0}$ is a 2×2 null matrices and $\boldsymbol{I}$ denotes a 2×2 identity matrix. The symbol E represents the statistical expectation operator and the superscript ^{H} means the Hermitian transpose operation. The matrix $\boldsymbol{P}_p^f$ in (8) is in its essence the

covariance matrix of the driving noise process for the forward AR(p) process.

The corresponding two-channel Yule-Walker equations for backward prediction can also be derived in a similar way as

$$\boldsymbol{b}_p \boldsymbol{R}_p = [\boldsymbol{0} \cdots \boldsymbol{0}\ \boldsymbol{P}_p^b], \tag{9}$$

in which

$$\boldsymbol{b}_p = [\boldsymbol{B}_p(p) \cdots \boldsymbol{B}_p(1)\ \boldsymbol{I}] \tag{10}$$

and

$$\boldsymbol{P}_p^b = E\{\boldsymbol{e}_p^b[n-1]\boldsymbol{e}_p^{bH}[n-1]\}. \tag{11}$$

The matrix $\boldsymbol{P}_p^b$ in (11) is the covariance matrix of the driving noise process for the backward AR(p) process.

The correlation matrix $\boldsymbol{R}_p$ in (6) has a Hermitian and a block-Toeplitz structure. By the definition, the correlation matrix at order p+1, $\boldsymbol{R}_{p+1}$, has the same structure, too. $\boldsymbol{R}_{p+1}$ can be partitioned in two ways

$$\boldsymbol{R}_{p+1} = \begin{bmatrix} \boldsymbol{R}_p & \boldsymbol{s}_{p+1}^H \\ \boldsymbol{s}_{p+1} & r_{xx}[0] \end{bmatrix} \tag{12}$$

or

$$\boldsymbol{R}_{p+1} = \begin{bmatrix} r_{xx}[0] & \boldsymbol{r}_{p+1} \\ \boldsymbol{r}_{p+1}^H & \boldsymbol{R}_p \end{bmatrix}, \tag{13}$$

in which

$$\boldsymbol{s}_{p+1} = \begin{bmatrix} r_{xx}[-p-1] & r_{xx}[-p] & \cdots & r_{xx}[-1] \end{bmatrix}, \tag{14}$$

and

$$\boldsymbol{r}_{p+1} = \begin{bmatrix} r_{xx}[1] & r_{xx}[2] & \cdots & r_{xx}[p+1] \end{bmatrix}, \tag{15}$$

with the definition

$$r_{xx}[k] \equiv E\{x[n] \cdot (x[n-k])^*\}. \tag{16}$$

The partitions in (12) and (13) may then be utilized to construct the following relationships

$$\begin{bmatrix} \boldsymbol{a}_p & \boldsymbol{0} \end{bmatrix} \boldsymbol{R}_{p+1} = \begin{bmatrix} \boldsymbol{P}_p^f & \boldsymbol{0} \cdots \boldsymbol{0} & \Delta_{p+1} \end{bmatrix}, \tag{17}$$

and

$$\begin{bmatrix} \boldsymbol{0} & \boldsymbol{b}_p \end{bmatrix} \boldsymbol{R}_{p+1} = \begin{bmatrix} \nabla_{p+1} & \boldsymbol{0} \cdots \boldsymbol{0} & \boldsymbol{P}_p^b \end{bmatrix}, \tag{18}$$

in which the 2×2 matrices Δ_{p+1} and ∇_{p+1} are defined as

$$\Delta_{p+1} = \boldsymbol{a}_p \boldsymbol{s}_{p+1}^H, \tag{19}$$

$$\nabla_{p+1} = \boldsymbol{b}_p \boldsymbol{r}_{p+1}^H. \tag{20}$$

Based on (17) and (18), and with the expansion of (4) and (9) to the order p+1, the following relationships can thus be derived

$$\boldsymbol{a}_{p+1}\boldsymbol{R}_{p+1} = \left([\boldsymbol{a}_p\ \boldsymbol{0}] + \boldsymbol{K}^f[\boldsymbol{0}\ \boldsymbol{b}_p]\right)\boldsymbol{R}_{p+1} = \left[\boldsymbol{P}_{p+1}^f\ \boldsymbol{0} \cdots \boldsymbol{0}\right], \tag{21}$$

$$\boldsymbol{b}_{p+1}\boldsymbol{R}_{p+1} = \left(\boldsymbol{K}^b[\boldsymbol{a}_p\ \boldsymbol{0}] + [\boldsymbol{0}\ \boldsymbol{b}_p]\right)\boldsymbol{R}_{p+1} = \left[\boldsymbol{0} \cdots \boldsymbol{0}\ \boldsymbol{P}_{p+1}^b\right]. \tag{22}$$

On the element-by-element checks in (21) and (22) and with the relationships (17)-(20), it can be appreciated that

$$\boldsymbol{K}^f = \boldsymbol{A}_{p+1}(p+1), \tag{23}$$

$$\boldsymbol{K}^b = \boldsymbol{B}_{p+1}(p+1), \tag{24}$$

and

$$\boldsymbol{A}_{p+1}(k) = \boldsymbol{A}_p(k) + \boldsymbol{A}_{p+1}(p+1)\boldsymbol{B}_p(p+1-k), \tag{25}$$

$$\boldsymbol{B}_{p+1}(k) = \boldsymbol{B}_p(k) + \boldsymbol{B}_{p+1}(p+1)\boldsymbol{A}_p(p+1-k), \tag{26}$$

for k=1 to p. Besides, the following relationships can also be acquired

$$\boldsymbol{A}_{p+1}(p+1) = -\Delta_{p+1}(\boldsymbol{P}_p^b)^{-1}, \tag{27}$$

$$\boldsymbol{B}_{p+1}(p+1) = -\nabla_{p+1}(\boldsymbol{P}_p^f)^{-1}, \tag{28}$$

and

$$\boldsymbol{P}_{p+1}^f = [\boldsymbol{I} - \boldsymbol{A}_{p+1}(p+1)\boldsymbol{B}_{p+1}(p+1)]\boldsymbol{P}_p^f, \tag{29}$$

$$\boldsymbol{P}_{p+1}^b = [\boldsymbol{I} - \boldsymbol{B}_{p+1}(p+1)\boldsymbol{A}_{p+1}(p+1)]\boldsymbol{P}_p^b, \tag{30}$$

for which $\boldsymbol{A}_{p+1}(p+1)$ and $\boldsymbol{B}_{p+1}(p+1)$ are the forward and backward reflection coefficients in the two-channel case.

Let $\boldsymbol{P}_p^{fb}$ be denoted as the cross correlation between the forward and backward prediction residuals at one unit of lag, that is

$$\boldsymbol{P}_p^{fb} = E\{\boldsymbol{e}_p^f[n]\boldsymbol{e}_p^{bH}[n-1]\}. \tag{31}$$

From the relationships (2)-(3) and (19)-(20), it can be proved that

$$\boldsymbol{P}_p^{fb} = \Delta_{p+1} = \nabla_{p+1}^H. \tag{32}$$

Substitute (32) into (27) and (28), the forward and backward reflection coefficients can be calculated by

$$\boldsymbol{A}_{p+1}(p+1) = -\boldsymbol{P}_p^{fb}(\boldsymbol{P}_p^b)^{-1}, \tag{33}$$

$$\boldsymbol{B}_{p+1}(p+1) = -(\boldsymbol{P}_p^{fb})^H(\boldsymbol{P}_p^f)^{-1}. \tag{34}$$

From the definition in (7), the data matrix of order p+1 is given by

$$\boldsymbol{x}_{p+1}[n] = \begin{bmatrix} \boldsymbol{x}_p[n] \\ \boldsymbol{x}[n-p-1] \end{bmatrix} = \begin{bmatrix} \boldsymbol{x}[n] \\ \boldsymbol{x}_p[n-1] \end{bmatrix}. \tag{35}$$

In addition, the following two relationships can be obtained from (21)-(24)

$$\boldsymbol{a}_{p+1} = [\boldsymbol{a}_p\ \boldsymbol{0}] + \boldsymbol{A}_{p+1}(p+1)[\boldsymbol{0}\ \boldsymbol{b}_p], \tag{36}$$

$$\boldsymbol{b}_{p+1} = \boldsymbol{B}_{p+1}(p+1)[\boldsymbol{a}_p\ \boldsymbol{0}] + [\boldsymbol{0}\ \boldsymbol{b}_p]. \tag{37}$$

The relationships of the driving noise process between AR(p) and AP(p+1) can be obtained by postmultiplying both (36) and (37) by $\boldsymbol{x}_{p+1}[n]$ to yield

$$\boldsymbol{e}_{p+1}^f[n] = \boldsymbol{e}_p^f[n] + \boldsymbol{A}_{p+1}(p+1)\boldsymbol{e}_p^b[n-1] \tag{38}$$

and

$$\boldsymbol{e}_{p+1}^b[n] = \boldsymbol{e}_p^b[n-1] + \boldsymbol{B}_{p+1}(p+1)\boldsymbol{e}_p^f[n]. \tag{39}$$

It is assumed that there are N samples in both sequences. The Vieira-Morf method is an order update recursion algorithm and is initialized by

$$\boldsymbol{P}_0^f = \boldsymbol{P}_0^b = \frac{1}{N}\sum_{n=1}^{N} \boldsymbol{x}[n]\boldsymbol{x}^H[n] \tag{40}$$

and

$$\boldsymbol{e}_0^f[n] = \boldsymbol{e}_0^b[n] = \boldsymbol{x}[n]. \tag{41}$$

The whole procedure of Vieira-Morf method is summarized in TABLE I.

For bivariate AR(P) power spectrum density (PSD), define the complex exponential vector $\boldsymbol{E}_P(f)$ of P+1 block elements as

$$\boldsymbol{E}_P(f) = [\boldsymbol{I}\ \exp(j2\pi fT)\boldsymbol{I} \cdots \exp(j2\pi fPT)\boldsymbol{I}], \tag{42}$$

in which T is the sampling interval (sec) of the signals $\boldsymbol{x}[\cdot]$. After the computation of the related coefficients, the PSD can be calculated by

$$\boldsymbol{P}_{AR}(f) = T[\boldsymbol{a}_P \boldsymbol{E}_P^H(f)]^{-1} \boldsymbol{P}_P^f [\boldsymbol{E}_P(f)\boldsymbol{a}_P^H]^{-1} = \begin{bmatrix} P_{11}(f) & P_{12}(f) \\ P_{21}(f) & P_{22}(f) \end{bmatrix} \quad (43)$$

where $\boldsymbol{a}_P$ is defined in (5).

The magnitude squared coherence (MSC)

$$C(f) = \frac{|P_{21}(f)|^2}{P_{11}(f)P_{22}(f)} \quad (44)$$

and the coherence phase

$$\theta(f) = \tan^{-1} \frac{\mathrm{Im}\{P_{21}(f)\}}{\mathrm{Re}\{P_{21}(f)\}} \quad (45)$$

versus frequency f are utilized for the coherence analysis between respiration and PPG signal in this research. In addition, the corresponding PSD of respiration and PPG signal can be derived from $P_{11}(f)$ and $P_{22}(f)$ versus frequency f.

III. Results and Discussion

The coherence between the measured PPG and respiratory signals at different breathing rates from ten subjects was analyzed to evaluate their relationships in frequency domain. Fig.2 shows the coherence analysis results for one subject in the condition of 12-breaths/min rate. As seen in Fig. 2(a), there exists MSC greater than 0.5 near 0.2 Hz (the respiratory frequency, see Fig.2(c)). Also, the coherence phase is smaller than zero (see Fig.2(b)), which imply that the respiration-induced changes in PPG signal lags the respiratory signal. It also can be appreciated that there is a corresponding component near the respiratory frequency in the PSD of PPG signal, as depicted in Fig.2(d).

The results in the 20-breaths/min condition for the same subject are demonstrated in Fig.3 with the same order arranged in Fig.2. The MSC depicts that high coherence exists between respiration and PPG signal (see Fig. 3(a)). Also, the respiration-induced change in PPG has a time delay compared with the respiratory signal, as shown in Fig.3(b).

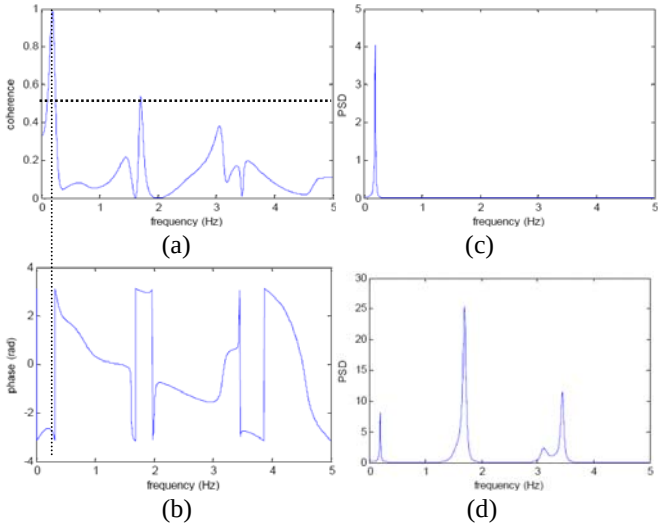

Fig. 2 Coherence analysis results in 12-breaths/min rate for one subject: (a) MSC, (b) coherence phase, (c) PSD of respiratory signal, and (d) PSD of PPG signal

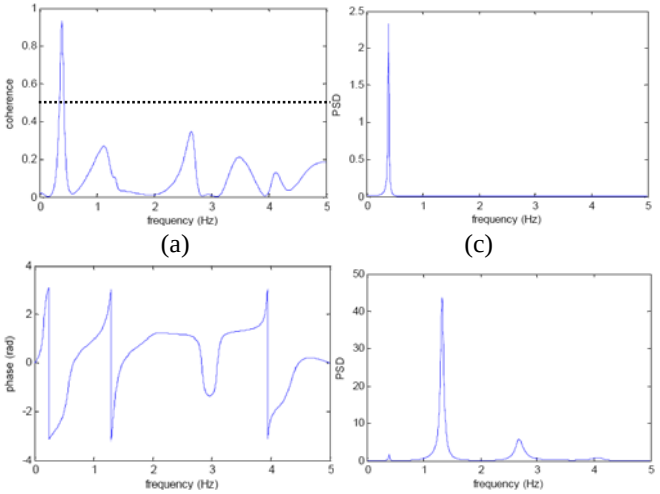

Fig. 3 Coherence analysis results in 20-breaths/min rate: (a) MSC, (b) coherence phase, (c) PSD of respiratory signal, and (d) PSD of PPG signal

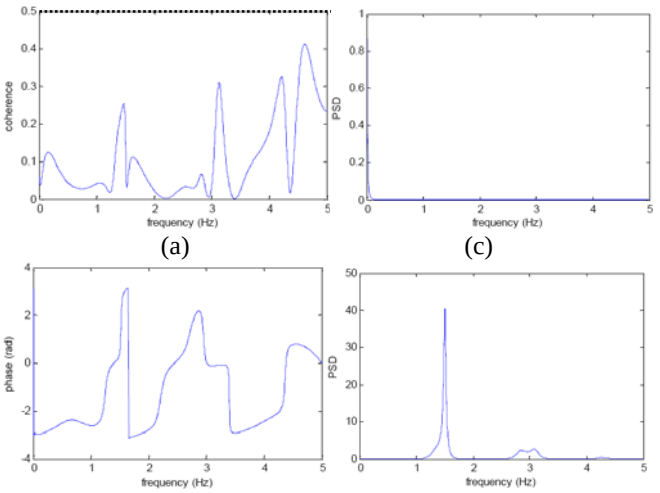

Fig. 4 Coherence analysis results in breath-holding condition: (a) MSC, (b) coherence phase, (c) PSD of respiratory signal, and (d) PSD of PPG signal

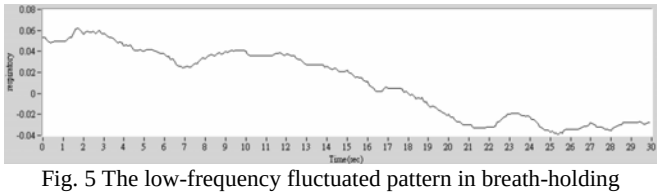

Fig. 5 The low-frequency fluctuated pattern in breath-holding condition for another subject

Fig.4 shows the results in holding-breath condition for the same subject. As all of the MSC values are less than 0.5 (see Fig.4(a)), it is appreciated that no coherence is found in such case.

Though only the results from one subject are depicted in this paper, similar results are derived for almost all subjects. The

only exception is the coherent result was found in the breath-holding condition for one subject. After checking the original respiratory signal, very low-frequency fluctuation was found and is demonstrated in Fig. 5. The reason may be due to the breath of the subject is not indeed in the holding status such that little airstream flows through the nostril during the experiment. For the cases without coherence in breath-holding condition, such fluctuation as that shown in Fig.5 is not evident.

From Fig.2(d) and Fig.3(d), there exists corresponding respiratory peak in the PSD of PPG signal. These components are usually much smaller compared with the dominant peaks which relate directly to the heart beats. If the Fourier-based techniques were applied in the research, the respiration-related component will not be as obvious as depicted in this research.

IV. Conclusion

This study utilized bivariate AR spectral estimation method to investigate the coherence between the respiratory signal and PPG signal under different respiratory rates. The Vieira-Morf method was used for the computation of bivariate AR parameters. The algorithm is summarized in TABLE I. The coherence analysis results are demonstrated in Fig.2-Fig.4. The results show that they are coherent (MSC greater than 0.5) at the respiratory frequency. In addition, the response delay in PPG induced by respiration is also implied in the negative coherence phase (see Fig.2(b) and Fig.3(b)). The respiration induced component is usually evident in the PSD of PPG signal, as shown in Fig.2(d) and Fig. 3(d). The coherence analysis is also specific to respiration. As the breath is in holding status, no coherent peak was found in almost all coherence analysis results (see Fig.4).

The existence of coherent peak can be determined by checking whether the corresponding pole inside the unit circle is prominent or not. It has been shown that the coherence spectrum is sensitive and specific to the respiration in this research. It may be possible to acquire the respiratory information from PPG signal by single-channel AR method with the consideration of poles around the respiratory frequency. Besides, the bivariate AR method introduced in section II can be easily expanded to more than three channels. Such multi-channel AR method may be an alternative attractive tool for the coherent analysis among respiration, central venous pressure (CVP), arterial blood pressure (ABP) and PPG signal in the related research, e.g. for the cases in intensive care unit (ICU) or during surgical operation.

Acknowledgment

The authors wish to express their appreciation to the National Science Council, Taiwan, for the financial support on this research (contract number NSC 97-2221-E-035-001-MY3 and NSC 97-2221-E- 035-053).

References

[1] A. B. Hertzman and C. R. Spielman, "Observations on the finger volume pulse recorded photoelectrically", *Am. J. Physiol.*, 1937, vol.119, pp.334-335.

[2] J. Allen, "Photoplethysmography and its application in clinical physiological measurement", *Physiol. Meas.*, 2007, vol.28, no.3, pp.R1-R39.

[3] R. D. Allison, E. L. Holmes and J. Nyboer, "Volumetric dynamic of respiration as measured by electrical impedance plethysmography", *J. Appl. Physiol.*, 1964, vol.19, pp.166-173.

[4] A. M. Cyna, V. Kulkarni, M. E. Tunstall, J. M. S. Hutchinson and J. R. Mallard, "Aura: a new respiratory monitoring and apnea alarm for spontaneously breathing patients", *Br. J. Anaesth.*, 1991, vol.67, pp.341-345.

[5] A. Johansson, P. Å. Öberg and G. Sedin, "Monitoring of heart and respiratory rates in newborn infants using a new photoplethysmographic technique", *J. Clin. Monit.*, 1999, vol.15, pp.461-467.

[6] L. Nilsson, A. Johansson and S. Kalman, "Monitoring of respiratory rate in postoperative care using a new photoplethysmographic technique", *J. Clin. Monit.*, 2000, vol.16, pp.309-315.

[7] A. Johansson and P. Å. Öberg, "Estimation of respiratory volumes from the photoplethysmographic signal. Part I: experimental results", *Med. Biol. Eng. Comput.*, 1999, vol.37, pp.42-47.

[8] A. Johansson and P. Å. Öberg, "Estimation of respiratory volumes from the photoplethysmographic signal. Part II: a model study", *Med. Biol. Eng. Comput.*, 1999, vol.37, pp.48-53.

[9] L. Nilsson, A. Johansson and S. Kalman, "Macrocirculation is not the sole determinant of respiratory induced variations in the reflection mode photoplethysmographic signal", *Physiol. Meas.*, 2003, vol.24, pp.925-937.

[10] M. Morf, A. Vieira, D. T. Lee and T. Kailath, "Recursive multichannel maximum entropy spectral estimation", *IEEE Trans. Geosci. Electron.*, 1978, vol.16, pp.85-94.

[11] S. L. Marple Jr., *Digital Spectral Analysis with Applications*. New Jersey: Prentice-Hall, 1987, ch.15.

[12] N. Levinson, "The Wiener RMS (root mean square) error criterion in filter design and prediction", *J. Math. Phys.*, 1947, vol.25, pp.261-278.

Yue-Der Lin (M'00-SM'07) was born in Taichung, Taiwan, in 1963. He earned the Ph.D. degree of electrical engineering from National Taiwan University in 1998. He has been a lecture of the Department of Electrical Engineering, Wufeng Institute of Technology in 1991 and 1992, and a teaching assistant in the Department of Electrical Engineering, National Taiwan University from 1996 to 1998. He joined Comtrend Corporation as a design engineer in 1998 and was responsible for the design of embedded systems in telecommunication. He joined the faculty of the School of Post Baccalaureate Chinese Medicine, China Medical College in 1999 as an assistant professor where his research efforts were focused on medical device design and biomedical signal processing. Since 2003, he became an associate professor at the Department of Automatic Control Engineering, Feng Chia University, Taichung, Taiwan. Dr. Lin is a visiting scholar of the University of Wisconsin-Madison in 2006, where he pursued the research in ECG signal processing. He is the winner of the *Rotary International Scholarship* in 1994-1995 and 1996-1997, and has been listed in *Marquis Who's Who in the World* in 2008 and 2009 for his researches on physiological signal analysis and wearable technology. He has also been listed in *IBC Top 100 Educators*, *2000 Outstanding Intellectuals of the 21st Century*, *Foremost Educators of the World*, *Foremost Engineers of the World*, *21st Century Award for Achievement* and *Leading Engineers of the World* in 2008.

Dr. Lin's research interests include the medical instrumentation, biomedical signal processing and statistical signal processing. He is a senior member of IEEE EMB society.

TABLE I
ALGORITHM FOR BIVARIATE AR PARAMETERS

Let $\boldsymbol{X} = [\boldsymbol{x}[1]\ \boldsymbol{x}[2]\cdots\boldsymbol{x}[n]\cdots\boldsymbol{x}[N]]$

and P = the order of bivariate AR model.

Initialization: $\begin{cases} \boldsymbol{e}_0^f[n] = \boldsymbol{e}_0^b[n] = \boldsymbol{x}[n] \quad for\ n = 1,2,\cdots N \\ \boldsymbol{P}_0^f = \boldsymbol{P}_0^b = \boldsymbol{X}\boldsymbol{X}^H / N \end{cases}$

Computation:

$p = 0$

while $p \le P$

$$\begin{cases} \boldsymbol{P}_p^f = \dfrac{1}{N}\displaystyle\sum_{n=p+2}^{N} \boldsymbol{e}_p^f[n]\boldsymbol{e}_p^{fH}[n] \\ \boldsymbol{P}_p^b = \dfrac{1}{N}\displaystyle\sum_{n=p+2}^{N} \boldsymbol{e}_p^b[n-1]\boldsymbol{e}_p^{bH}[n-1] \\ \boldsymbol{P}_p^{fb} = \dfrac{1}{N}\displaystyle\sum_{n=p+2}^{N} \boldsymbol{e}_p^f[n]\boldsymbol{e}_p^{bH}[n-1] \end{cases}$$

$p = p+1$

$$\begin{cases} \boldsymbol{A}_{p+1}(p+1) = -\boldsymbol{P}_p^{fb}\left(\boldsymbol{P}_p^b\right)^{-1} \\ \boldsymbol{B}_{p+1}(p+1) = -\left(\boldsymbol{P}_p^{fb}\right)^H \boldsymbol{P}_p^{f\ -1}\ (\quad) \end{cases}$$

$$\begin{cases} \boldsymbol{P}_{p+1}^f = [\boldsymbol{I} - \boldsymbol{A}_{p+1}(p+1)\boldsymbol{B}_{p+1}(p+1)]\boldsymbol{P}_p^f \\ \boldsymbol{P}_{p+1}^b = [\boldsymbol{I} - \boldsymbol{B}_{p+1}(p+1)\boldsymbol{A}_{p+1}(p+1)]\boldsymbol{P}_p^b \end{cases}$$

for $k = 1,2,\cdots p-1$

$$\begin{cases} \boldsymbol{A}_{p+1}(k) = \boldsymbol{A}_p(k) + \boldsymbol{A}_{p+1}(p+1)\boldsymbol{B}_p(p+1-k) \\ \boldsymbol{B}_{p+1}(k) = \boldsymbol{B}_p(k) + \boldsymbol{B}_{p+1}(p+1)\boldsymbol{A}_p(p+1-k) \end{cases}$$

end for

for $n = p+1, p+2, \cdots N$

$$\begin{cases} \boldsymbol{e}_{p+1}^f[n] = \boldsymbol{e}_p^f[n] + \boldsymbol{A}_{p+1}(p+1)\boldsymbol{e}_p^b[n-1] \\ \boldsymbol{e}_{p+1}^b[n] = \boldsymbol{e}_p^b[n-1] + \boldsymbol{B}_{p+1}(p+1)\boldsymbol{e}_p^f[n] \end{cases}$$

end for

end while